BDH Universal Liquid Indicator was used to measure pH on unfiltered waters at the site of collection where possible.

V ATOMIC ABSORPTION SPECTROPHOTOMETRY

The theory and interference problems associated with atomic absorption spectrophotometry as an analytical tool are adequately discussed elsewhere (Abbey, 1967; Christian and Feldman, 1970; Fletcher, 1970). A techtron AA4 atomic absorption spectrophotometer was used for Ca, Cu, Fe, Mg, Mn and Zn determinations, and a Perkin-Elmer 303, equipped with a deuterium continuum lamp for background correction, was used for determinations of Ag, Cd, and Pb.

Samples were analyzed in batches of 24; each batch included a U.B.C. standard rock sample, an analytical blank, and a duplicate sample. Chemical interferences in the determination of Ca and Mg in soil were reduced by addition of a lanthanum oxide solution as a releasing agent (Christian and Feldman, 1970, pp. 237-258). This procedure was not taken with water samples and these results, therefore, are not absolute. Instrumental procedures as described by Fletcher (1971) were followed and are presented in Table 3.

Table 3. Operating conditions for the Techtron AA4 and Perkin-Elmer 303 atomic absorption spectrophotometers.

Element	Current (ma)	Fuel Gauge	Air Pressure	Slit Width	Wavelength (A°)
Ag[1]	6	4.0	5.0	1 mm	3280
Ca	10	3.5	20.0	100µ	4227
Cd[1]	6	4.0	5.0	1 mm	2288
Cu	3	2.5	20.0	50µ	3248
Fe	5	2.5	20.0	50µ	3720
Mg	4	3.5	20.0	100µ	2852
Mn	10	2.5	20.0	100µ	2795
Pb[1]	14	4.0	5.0	1 mm	2175
Zn	6	2.3	20.0	100µ	2139

1: Elements determined on the Perkin-Elmer 303, air and fuel flow rates are based on arbitrary scales for all elements.

VI MISCELLANEOUS ANALYTICAL TECHNIQUES

A. Size Fraction Analysis

Approximately 65 g of disaggregated dry soil was placed in a set of stainless steel sieves (U.S. Standard No. 10, 40, 80 and 270)[1] and shaken on a rotap for five minutes. Results are expressed in weight percent of the minus 10-mesh fraction.

B. Heavy Mineral Separates

Heavy minerals were separated from 1 g samples of minus 80-plus 270-mesh material using bromoform, specific gravity 2.89. Each sample was shaken with bromoform and allowed to settle for 10 minutes before the heavy fraction was drained off. This procedure was repeated two to three times rinsing the sides of the funnel free of mineral grains after each shaking. Results are expressed in milligrams per gram. Trace element analysis of heavy mineral separates followed the same procedure as used for soil samples using a 4:1 nitric-perchloric acid digestion.

C. Conductivity and pH

Sample pH was determined by placing 5 g pebble-free samples, into paper cups and adding 25 ml of distilled water.

1: Metric mesh sizes of 2.0, 0.42, 0.177 and 0.053mm respectively.

The resulting slurries were stirred three to four times over a one hour period, before measuring pH with an Orion 404 pH meter. Electrodes were occasionally calibrated using buffered solutions of pH 4.0 and 9.0.

Conductivity measurements, using a Hach 2510 conductivity meter, were made on the same slurries after addition of a further 25 ml of distilled water. The slurries were stirred and allowed to settle for one-half hour before a final stirring at the time of measurement. Values are presented as microhms per square centimeter with a 1:10 soil to water mixture.

D. Loss on Ignition

Loss on ignition (L.O.I.) was used to estimate organic content of 60 lake sediment samples. Approximately 1g (0.6 to 1.5g) samples were weighed in crucibles and placed in a muffle furnace. The temperature was gradually raised over an hour to 500^{o}C, held at this temperature for three hours, followed by a 3 to 5 hour cool down. The crucibles were then reweighed and the percentage weight loss recorded.

VII ANALYTICAL PRECISION

Analytical control and precision was maintained with an analytical blank and a U.B.C. standard rock sample. Precision was estimated by analysis of paired samples and by replicate

Table 4. Precision estimates at the 95 percent confidence level for paired soil samples and replicate standard rock analyses by atomic absorption spectrophotometry.

Element	Average Concentration[1]	No. of Paired Samples	Precision (±%)
Ag	1.04 (d.l.)[2]	42	69
Ca	514 (5240)	10 (7)	15 (16)
Cd	0.96 (d.l.)	42 (40)	21
Cu	125 (22)	42 (40)	10 (17)
Fe	2.51% (1.53%)	42 (40)	20 (23)
Mg	1.04% (0.52%)	10 (7)	18 (25)
Mn	350 (262)	42 (41)	5 (7)
Pb	283 (d.l.)	42 (41)	13
Zn	230 (14)	42 (41)	19 (17)

1: Concentration in parts per million (ppm) unless otherwise noted.

2: () results for the U.B.C. standard rock.

d.l.: Signifies concentration levels below the detection limit.

Table 5. Precision estimates at the 95 percent confidence level for paired sediment samples analyzed by atomic absorption spectrophotometry.

Element	Average Concentration[1]	No. of Paired Samples	Precision (±%)
Ag	0.52	8	23.4
Cd	5.90	8	1.7
Cu	1130.0	8	6.4
Fe	4.2%	8	6.1
Mn	5055.0	8	17.5
Pb	187.0	8	4.2
Zn	1466.0	8	6.2

1: Concentration in parts per million (ppm) unless otherwise noted.

analysis of the U.B.C. standard rock. Precision on these samples at the 95 percent confidence level was computed on an IBM 360/67 computer according to a procedure outlined by Garrett (1969) and programed by Fox (1971). Results for paired samples and replicate analyses are presented in Tables 4 and 5 respectively. Except for Zn, precision values for the standard rock are very close to, but consistently poorer than, those determined for the paired soil samples. Unfortunately, precision values for Ag, Cd, and Pb for the standard rock are not available because concentrations of these elements lie below the detection limit.

Comparison of Tables 4 and 5 shows that precision for sediments is better than for soils, except for Mn. This most likely reflects the smaller grain size of the sediments and the greater ease and completeness of the digestion relative to the soils. In the case of Mn, poor precision within the sediments may be caused by manganese's irregular distribution (Bolviken and Sinding-Larsen, 1973, p. 295) where values range from 300 to in excess of 80,000 ppm.

Duplicate water samples were not collected and analytical precision cannot therefore be estimated; however, multiple samples taken from Camp Lake at different times show a remarkable similarity (Table 6). Cameron and Ballantyne (1975) and Cameron (1977b) also report little to moderate variation in metal content with time in samples they collected and analyzed. Furthermore, metal concentrations in lake waters

Table 6. Comparison of Zn concentrations (ppb) in samples collected from Camp Lake in July 1974 and 1975 and from Anne Lake in 1974.

Camp Lake		Anne Lake
1974	1975	1974
74	65	33
69	74	37
72	71	37
74	71	37
74	71	46
71	68	
$\bar{X}$=72	$\bar{X}$=70	

Copper was below the detection limit (≈15 ppb) in all samples.

Table 7. Comparison of Zn and Cu concentrations (ppb)[1] in lake waters as a function of time and analytical technique.

Lake	Zn[2]			Cu[2]		
	A	B	C	A	B	C
Camp[3]	72	71	69	<15	9	<15
Banana[3]	<10	4	<10	<15	2	<15
Anne[3]	38	44		<15	6	
Lower Sunken	28	30		<15	2	
Upper Sunken	63	63		<15	8	
Flying Horse	355	404		<15	27	
Turtle[3]	11	16		<15	3	
Cleaver	118	166		<15	5	

1: Detection limits: this study 15 ppb Cu, 10 ppb Zn; Cameron et. al. (1975) 1 ppb for Cu and Zn.

2: A: Data from this study, 1974.
B: Data from Cameron et. al., 1975 (collected in 1974).
C: Data from this study, 1975.

3: Average of more than one sample.

collected by this author in 1974 and 1975 are similar, even though a different analytical technique was used, to values reported by Cameron and Ballantyne (1975) as shown in Table 7.

Because of the low number of paired samples for each type of partial extraction and size fraction analyzed, precision was assessed using a graphical method developed by Thompson and Howarth (1973) and shown in Figure 20. Precision at the 90 percent confidence level, except for low levels of Pb, closely conforms to an arbitrarily chosen precision limit of $\pm$20 percent. In addition, data for duplicate samples subjected to size fraction analysis, L.O.I. and heavy mineral separations shows that analytical precision of these three procedures is within $\pm$10 percent of the original value. Results are therefore considered more than adequate for the purposes of this thesis.

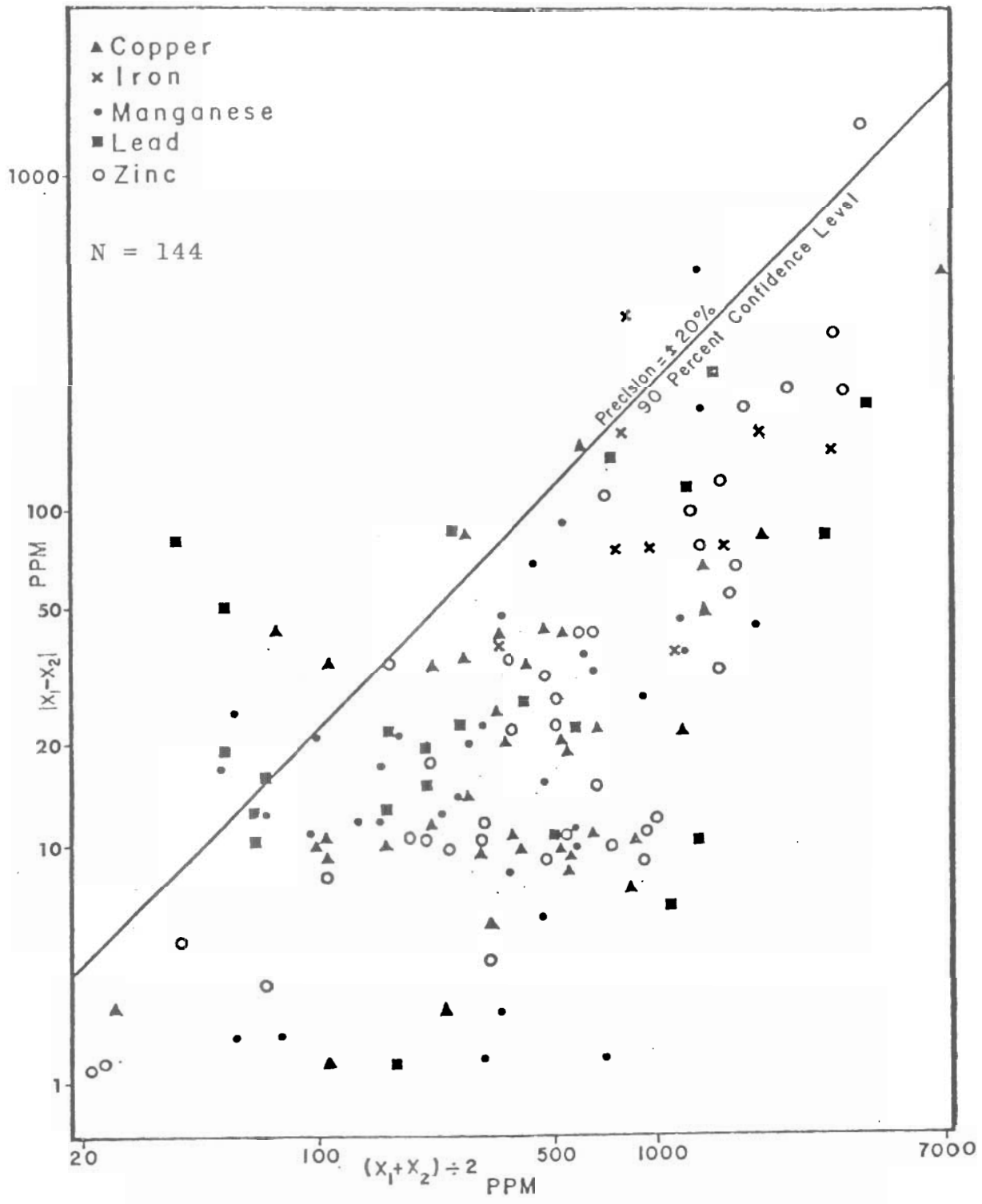

Figure 20. Precision conformation at the 90th percentile for an arbitrarily chosen precision of ± 20% (after Thompson and Howarth, 1973). Data are paired samples of various size fractions, subjected to several partial attacks.

CHAPTER 4

PRESENTATION OF ANALYTICAL DATA

I INTRODUCTION TO DATA PRESENTATION

Due to the volume of geochemical data in the form of figures for Chapter 4 it has become necessary to assemble these figures at the end of the chapter. The various tables remain within the text as in previous chapters.

Geochemical data for the soil grid are divided into three soil layers: an easily identifiable organic-rich soil horizon (L-F-H) and two arbitrarily chosen mineral soil layers (0 to 14 inch and 14 to 25 inch; hereafter referred to as Layer 1 and Layer 2 respectively). Each of the three layers is presented as several single element contour maps prepared from computer plots. Contour intervals were selected on the basis of computer derived log-normalized histograms and/or probability plots prepared from histograms following the methods of Lepeltier (1969) and Sinclair (1976). In some cases (e.g. Fe and Cu) contour intervals vary between soil layers as a result of fluctuating metal values with depth and/or because the most precise intervals, in terms of pattern development, were sought.

For the contoured geochemical maps, thresholds (i.e. anomalous vs background) are not shown because the majority of the data for many of the elements can be considered

anomalous on a regional scale, although not readily apparent in this study. Because of the scale of this study, local thresholds (more highly anomalous concentrations) are more important and are discussed in somewhat limited detail. Nevertheless, this author prefers to emphasize pattern development rather than 'high numbers' when relating geochemical anomalies to a bedrock source. This is based on the knowledge that in glaciated areas near-surface soil geochemical anomalies may be displaced down ice considerable distances resulting in highly anomalous values overlying barren bedrock while less anomalous, possibly background, values overlie mineralization. Therefore, pattern development is of prime importance.

The deep soil pit data (multi-element graphs, size fractions, pH, conductivity, partial attacks and heavy mineral analysis) are considered in Section III and, except for several selected examples, the remainder of the data has been relegated to Appendix A. This is due partly to the volume of data and it's complexity which prevents making anything but broad generalizations. A discussion of all the soil data can be found in Chapter 5.

Dispersion in various water types (stream, lake, seepage, snow-melt runoff, etc.) as well as lake and stream sediments, was also investigated. Metal concentrations in these media reveal significant hydromorphic dispersion for several elements with Cu and, particularly, Zn the most notable.

Presentation of metal concentrations and patterns in waters and sediments are considered in Sections IV and V respectively. A general discussion of geochemical dispersion with respect to soil, water and sediment forms the basis of Chapter 5.

II SOILS

A. Probability Plots

Probability plots for Cu, Fe, Mn, Pb and Zn are presented with all three soil layers plotted on the same diagram (Figs. 21 to 25), although originally each soil layer was plotted separately. Superimposing the three soil layers facilitates identification of differences and similarities between the soil layers. Due to insufficient data, probability plots for Ag and Cd were not attempted.

Examination of the plots readily reveals that the distribution of metal values for most elements over most of the concentration range closely approximates a lognormal distribution; however, there are significant departures from a lognormal approximation, especially in the case of Fe, Mn, and, to a lesser extent, Cu, Pb and Zn. For Fe and Mn departure from lognormality occurs at high concentrations; whereas, for Cu, Pb and Zn it occurs only at low to very low concentrations.

Except for Mn (Fig. 23), variation between soil layers is minimal. In many cases one line or a smooth curve could be fitted to the data points to easily represent all three soil layers over most of the concentration range (e.g. Fe, Fig. 24).

In the case of Fe there is virtually no variation between soil layers; nevertheless, there is a distinct bi-modal distribution present which is clearly relatable to mineralization (Figs. 33 to 35). Following the method of Sinclair (1976) partitioning of either of the three Fe plots reveals two distinct populations with a well defined inflection point (optimum population separation) at ≈1.8 percent Fe (Fig. 22). Population A (anomalous) comprises 25 to 35 percent of the data with population B (background) the remainder. Parameters of partitioned populations A and B are given in Table 8.

The use of ≈1.8 percent Fe as a threshold (or 2 percent in the case of mineral soil Layers 1 and 2) proved most effective in outlining anomalous Fe concentrations (Figs. 33 to 35). The use of higher threshold values (e.g. 3%) were found to unduly restrict the extent of the anomaly, while lower threshold values (e.g. 1.5%) yielded nebulous, spotty patterns.

It was recognized at the outset of this thesis that the soil grids were strongly biased with respect to geochemical anomalies resulting in 30 to over 90 percent of the samples

Table 8. Parameters of partitioned lognormal Cu, Fe, Mn, Pb and Zn populations.

Population	Proportion	N^2	$\overline{X}^3$	σ^4	$\overline{X}+1\sigma$	$\overline{X}-1\sigma$
		Cu(ppm) Layer 1				
A	90	244	64(1.81)	0.46	185	23
B	10	37	10.5(1.02)	0.13	14	8
		Cu(ppm) Layer 2				
A	80	125	98(1.99)	0.47	290	33
B	20	32	16(1.20)	0.14	22	11.5
		% Fe^1				
A	≈32	226	2.1(0.32)	0.43	5.8	0.8
B	≈68	482	1.1(0.04)	0.14	1.5	0.8
		Mn(ppm) L-F-H				
A	38	103	98(1.99)	0.49	300	32
B	55	149	89(1.95)	0.07	103	76
C	7	19	27(1.43)	0.24	47	15.5
		Mn(ppm) Layer 1				
A	3.5	10	380(2.58)	0.24	660	220
B	96.5	271	120(2.08)	0.18	182	82

Cont/....

Population	Proportion	N^2	$\overline{X}^3$	σ^4	$\overline{X}+1\sigma$	$\overline{X}-1\sigma$
			Pb(ppm) L-F-H			
A	89	198	42(1.62)	0.56	155	11.5
B	11	25	4.8(0.68)	0.08	6.0	4.0
			Pb(ppm) Layer 1			
A	60	118	100(2.0)	0.86	730	14
B	40	78	5.8(0.76)	0.23	9.7	3.4
			Pb(ppm) Layer 2			
A	60	68	38(1.58)	0.94	330	4.4
B	40	45	5.8(0.76)	0.23	9.7	3.4
			Zn(ppm) Layer 1			
A	≈95.5	268	68(1.83)	0.35	150	30
B	≈4.5	13	22.5(1.35)	0.13	30	16.5

1: The Fe probability plots for the three soil layers have been combined and treated as one because of their close resemblance.

2: N = total number of samples in each population.

3: $\overline{X}$ = geometric mean followed by $\log_{10}\overline{X}$ in ( ).

4: σ = standard deviation in base 10 logorithms.

containing at least one metal in anomalous concentrations. Consequently, had the 'standard procedure' of the mean plus two standard deviations (cf. Hawkes and Webb, 1962) been chosen to define thresholds (e.g. 5.7% Fe), anomalies would have been reduced to a few small patches which - although pinpointing mineralized outcrops and float - would have greatly reduced the amount of information available (e.g. glacial smearing of Fe-rich till would have been mostly hidden within the background population).

Probability plots for Mn (Fig. 23) are somewhat more complex than for Fe, in that, a well developed trimodal distribution present in the L-F-H becomes a well developed bimodal distribution in Layer 1 and a unimodal distribution in Layer 2. Coupled with this is a distinct difference in the distribution of Mn between the mineral soil (Layers 1 and 2 have almost identical plots) and the organic-rich soil (L-F-H horizon). This difference is characterized by a relatively lower average concentration and wider range (steeper slope) of Mn values in the L-F-H horizon relative to the mineral soil (Table 9).

Partitioning of the trimodal and bimodal Mn probability plots (L-F-H and Layer 1 respectively) into their respective population groupings (see Table 8 for population parameters) reveals that in the L-F-H horizon, population A (anomalous) is associated with areas that are, for the most part, swampy (compare Figs. 15 and 36) or at the base of slopes (i.e. near

Table 9. Metal content[1] of soil at Camp Lake (minus 80-mesh fraction HNO_3/$HClO_4$ digestion).

Soil Layer		Ag[3]	Cd[4]	Cu	%Fe	Mn	Pb	Zn
	A	d-34	d-7.2	4-3720	0.3-25	14-3567	d-3088	9-682
L-F-H	B	1.7(.44)	1.2(.35)	61(.58)	1.37(.31)	89(.33)	36(.61)	71(.36)
N=270[2]	C	185	143	0	0	0	47	0
Layer 1	A	d-99	d-1.3	6-990	0.6-24	14-638	d-4600	14-422
0-14 in.	B	1.9(.61)	0.3(.30)	53(.50)	1.53(.24)	125(.19)	23(.71)	65(.30)
N=281	C	217	247	0	0	0	85	0
Layer 2	A	d-27	d-0.9	8-1021	0.3-20	66-473	d-4225	17-500
14-25 in.	B	2.6(.52)	0.5(.34)	67(.50)	1.65(.28)	129(.18)	35(.82)	66(.28)
N=157	C	110	133	0	0	0	44	0

A: Range.

B: Geometric mean followed by standard deviation (σ) in base 10 logs in ( ).

C: Number of samples below the detection limit, omitted from calculations of $\bar{X}$ and σ.

d: Detection limit: Ag ≈0.4 ppm; Cd ≈0.3 ppm; Pb ≈4.0 ppm.

1: Metal content in ppm unless noted otherwise.

2: N = total number of samples.

3: For Ag N = 262 L-F-H; 273 Layer 1 and 139 Layer 2.

4: For Cd N = 258 L-F-H; 269 Layer 1 and 145 Layer 2.

Camp Lake). In either case, pH is relatively high (compare Figs. 46 and 36). Although Eh was not measured, it is assumed to be high (oxidizing) because the underlying near surface mineral soil does not appear to be gleyed.

Conversely, population C, which is confined to the L-F-H horizon, is composed of very low Mn values ($\bar{X}$ = 27 ppm) which are associated with very acidic conditions and/or swampy areas where Eh is reducing (i.e. underlying mineral soil is strongly gleyed). In a few cases population C is associated with areas of relatively good internal drainage (i.e. Brunisols, compare Figs. 36 and 16). Although there is a wide range in Eh/pH conditions under which population C type values can be found, these conditions are such that Mn would be mobile and hence relatively depleted in relation to other areas within the L-F-H horizon.

As expected, population B occurs where environmental conditions are more normal, that is, Eh/pH is neither relatively high nor low and internal soil drainage is average. Consequently, population B comprises the largest percentage of the data. In the surficial soil, the percentage of population A relative to population B sharply decreases with depth (pop. A ≈38% L-F-H; ≈3.5% Layer 1) such that in Layer 2, whose plot is virtually a straight line, population A is not recognized.

As previously mentioned, the soil grids are strongly biased towards geochemical anomalies revealed in an earlier

soil survey by Cominco Limited. Consequently, the majority of soil samples contain relatively anomalous concentrations of Cu, Pb and Zn derived from mineralized bedrock. As a result, Cu, Pb and Zn are best approximated (at 95% confidence level) over most of the concentration range by single log-normal populations composed of anomalous values. However, the soil grid also contains a small to moderate percentage of samples (10 to 20% for Cu and Zn and 11 to 40% for Pb) with metal concentrations representative of background. The combination of Cu, Fe, Pb and Zn from two distinct sources (massive sulphides and non-mineralized bedrock) results in probability plots which are distinctly bimodal.

The degree of bimodality and the ease with which populations may be separated correlates with metal mobility. For example, highly mobile Zn exhibits the most linear probability plots of the three elements (Cu, Pb and Zn) and shows the least tendency towards bimodality; whereas, Pb, the least mobile of the three elements, displays the highest tendency towards bimodality and is also the least linear. Moderately mobile Cu, as expected, lies between Pb and Zn in terms of both linearity and bimodality.

In the case of Pb, relatively well developed anomalous (A) and background (B) populations can be defined with inflection points at the 60th and 89th cumulative percentiles (Layers 1 + 2 and L-F-H respectively). However, much of the background population (B) lies near the analytical detection

limit. Furthermore, Pb values recorded as zero ppm have been omitted from calculations and subsequent plots. Consequently, population B is not as precisely defined as A.

The relative importance of omitting the Pb data recorded as 'zero ppm' was assessed by: 1) inclusion of the data recorded as zero, recalculating percentages and reconstructing probability plots and 2) assuming that zero ppm Pb did not exist and that the samples actually contain 1 to 3 ppm Pb, a likely possibility (Hawkes and Webb, 1962, p. 367). Values of 1 to 3 ppm were then assigned (with 3 ppm emphasized over 2 ppm and so on), cumulative percentages recalculated and probability plots reconstructed. Results for the latter are shown for Layer 1 in Figure 24. In general, the latter assumption results in a better defined inflection point and easier population separation due to the inherent 'bottom limit' imposed by the 1 ppm boundary. Inclusion of the Pb values recorded as zero ppm results in a plot which is similar to the original plot but with population B no better defined than in the original plot.

Pb values in population B are characterized by the probability plot as less than 9 ppm in the L-F-H horizon and less than 22 ppm in mineral soil (Fig. 24). Applying these thresholds (rounded to the nearest ten for convenience) to the Pb soil grid data (Figs. 39 to 41) reveal that in the mineral soil the 20 ppm contour provides excellent separation between populations. Likewise, the 10 ppm contour for Pb in the

L-F-H horizon provides good population separation, although 20 ppm may be a better choice.

For Cu and Zn (Figs. 21 and 25) the presence of bimodal distributions are developed best in the mineral soil with Cu displaying less overlap between populations than Zn. Although there is a bimodal tendency in the L-F-H horizon, the high degree of overlap and the relatively small percentage ($\leq$6%) of data belonging to population (B) are such that separation is not warranted. Population B in Layer 1 can be assumed to roughly approximate population B for the L-F-H horizon based on the close similarity between the L-F-H horizon and Layer 1 probability plots for Cu and Zn at low metal concentrations. As with Pb, the upper limit of population B for Cu and Zn closely approximates the initial contour interval for the soil grid geochemical maps (Figs. 30 to 32 and 42 to 44) which in turn approximates the regional threshold.

In Figure 25, only population B for Zn (Layer 1) is shown because population A lies very close to the probability plot for the total data (as does population A for the L-F-H and Layer 2). A similar situation exists for Cu whereby population A (Layer 1 and L-F-H horizon) closely follows the trend shown by the probability plots for the respective total data and are not, therefore, presented.

In summary, probability plots for Cu, Fe, Mn, Pb and Zn were found to be useful in selecting contour intervals and

relating/defining grouped concentrations with possible sources and/or causes. They also aided, with regards to thresholds, in substantiating what may have been otherwise a subjective decision, especially where bimodal distributions are present but not readily recognizable in histogram form.

B. Nitric-perchloric Extraction Patterns

Except east of Camp Lake where a north-south orientation can sometimes be seen (e.g. Cu, Figs. 30 and 31; Zn Figs. 42 to 44), geochemical patterns - coinciding with the general strike of the geology and outcrops of footwall disseminated mineralization (Fig. 18) - display a general east-west trend. The former trend, which might result from line bias, is complicated by the presence of a veneer of glaciofluvial sediments. Anomalous geochemical patterns are best developed north of Camp Lake where they coincide with the general direction(s) of glaciation (Fig. 14) and the gossan zone (Fig. 45).

The most striking geochemical patterns are shown by Pb in Layers 1 and 2 where values increase from less than 20 ppm along the grid periphery to over 1000 ppm closer to mineralized zones (Figs. 18 and 39 to 41). In the L-F-H horizon, mineralized outcrops are adjacent to and contained within the 20 ppm contour. The 80 ppm contour is divided into two westward broadening zones, which are open at the western grid

limit, and separated by an east-west trending belt of lower values (<80 ppm) near the grid center. The southern belt closes sharply around mineralized outcrop east of B-C stream while the northern belt closes 200 to 300 feet west of mineralized outcrop near Banana Lake. Relative to the southern anomaly, the northern anomaly is broader, longer and more irregular.

The narrow belt of low (40 to 70 ppm) Pb values noted in the L-F-H horizon has broadened in Layer 1, effectively separating and providing better definition of the two east-west to west-northwest trending anomalies as now defined by the 100 ppm contour. It should be noted that broadening of this belt of low Pb values is not a function of the change in contour interval from 80 to 100 ppm because Pb values almost invariably lie below 70 ppm within this belt. In addition, there is a finger-like zone of high ($\geq$100 ppm) Pb with a southwest orientation associated with the northern Pb anomaly which is best developed in Layer 1 (Fig. 40).

Both of the Pb anomalies ($\geq$100 ppm) in Layer 1 lie on the outer flanks of the "mineral horizon" (Figs. 40 and 18) and can be related (particularly the southern anomaly) to mineralized outcrop adjacent to the B-C stream. However, for the northern Pb anomaly the relationship to mineralized outcrop is best defined in Layer 2 (Fig. 41).